12th HSTAM International Congress on Mechanics
Thessaloniki, Greece, 22 – 25 September 2019

NUMERICAL ANALYSIS FAILURE PREDICTION OF CFRP STIFFENED PANELS IN THE CONTEXT OF OPTIMAL AIRFRAME STRUCTURAL PERFORMANCE

Ioannis K. Giannopoulos [1*], Nicolae A. Bleoju [1], Ilias Tourlomousis [2], Efstathios E. Theotokoglou [2]

[1] Centre of Excellence for Aeronautics, School of Aerospace, Transport and Manufacturing, Cranfield University, Cranfield, MK43 0AL, UK
-mail: i.giannopoulos@cranfield.ac.uk ; web page: https://www.cranfield.ac.uk ; https://www.linkedin.com/in/adrianbleoju

[2] School of Applied Mathematical and Physical Sciences, Department of Mechanics Laboratory of Testing and Materials, The National Technical University of Athens, Zographou Campus, Theocaris Bld., GR-157 73, Athens, Greece
email: stathis@central.ntua.gr; webpage: http://www.semfe.ntua.gr/el/faculty-members/theotokoglou

Keywords: Composite structures, stiffened panel; progressive damage analysis, failure prediction

Abstract. *This paper presents the effect of stiffener damage on Carbon Fibre Reinforced Composite (CFRP) stiffened panels subjected to compression, for various stiffener design configurations. Nonlinear finite element progressive damage numerical simulations were used for the analysis. The investigation targeted the percentage decrease of the panel compression strength between the pristine (undamaged) and damaged stiffened panel states. The three designed cases sought, were assuming stiffened panels of the same weight but of different stiffener design. The study aimed at displaying that for CFRP stiffened panels used in aircraft structures and designed to carry loads where material strength could be the driver for the maximum compression loading capacity and not the structure's resistance to buckling, the stiffener geometry and material damage propagation are some of the major parameters for optimal stiffened panel design. In that regards and for cost saving from expensive testing surveys, nonlinear finite element analysis is a valuable tool for preliminary design studies and optimal design down-selection.*

---

*Corresponding author

Email: i.giannopoulos@cranfield.ac.uk; Tel: +44 (0) 1234 754692

1 INTRODUCTION

The aerospace industry has evolved and has embraced the adaptation of composites even on large civil transport airliners since the decisions of major aircraft manufacturers to build composite material airframes. These aircraft managed to achieve great efficiency by using several state-of-the-art technologies, including lightweight composite materials that account for over 50% of the aircraft Operational Empty Weight (OEW) [1].
The aerospace industry's change towards composite airframe structures was beneficial from many aspects, including environmental. One of the reasons why such materials were not extensively used by commercial and civil aviation much earlier, was the lack of sufficient research and in-service experience in their behaviour and performance. Despite their ability to reduce structural weight, civil airliner OEMs were allowed to use composites only in a rather reserved manner, as the airworthiness certification agencies and authorities responsible for ensuring flight safety had rigid standards that the composite structures would have to fulfil in order to achieve airworthiness certification. Therefore, for the past decades, considerable efforts have been allocated to research composite structures for airframe usage. Among many others, projects funded by the European Commission such as POSICOSS [2] and COCOMAT [3] have managed to create a broad experimental database for the purpose of structural performance validation.
Traditional lightweight airframe structures are made of structural thin sheets reinforced by stiffeners directed along the loading direction. Generally, those stiffened panel constructions as they are broadly referred to, suffer under compression loading more, hence are prone to buckling failure. Stiffened panels exhibit various bucking modes, differentiated as local or global depending on the location and the extent the structure is affected. The airworthiness regulations are distinguishing between two static load levels, the limit and ultimate loads [4]

against which certain structural performance criteria have to be attained and proven. Oversimplifying the respective clauses from such regulations and for civil aircraft, Limit Loading (LL) is the maximum loading to be experienced in service under the application of which the structure will not exhibit signs of detrimental deformation. Ultimate Loading (UL) is the magnified Limit Loading by a factor of 1.5 for civil airframes, under the application of which the structure must not fail. The interpretation of "detrimental deformation" and "failure" may vary according to the component's mission and location on the airframe. On many instances signs of early local buckling failure can be accepted to take place even below the LL condition as long as the rest of the performance criteria could be met. The response of the structure past initial buckling is termed post-buckling behaviour.

The POSICOSS project's objective was to output a series of procedures for reliable numerical simulations and design guidelines regarding the post-buckling behaviour of thin-walled Carbon Fibre Reinforced Plastic (CFRP) stiffened panels. The project concluded also that structural degradation could happen, during the post-buckling regime, before UL and final structural collapse. However, POSICOSS conclusions were based on simulations that only took into account geometrical nonlinearities without considering the structural degradation outset effect on the collapse of CFRP stiffened panels.

The COCOMAT project, as a follow on to POSICOSS, among other objectives, targeted to fill the gaps and establish much more accurate and reliable simulations of collapse to facilitate diverse design scenarios. Despite the advantages of using CFRP materials for stiffened panel constructions due to their high specific stiffness and strength, one considerable drawback is the induced damage which leads to significantly lower residual strength than their pristine condition. This implies the early onset of degradation and deviates from the design scenario developed by COCOMAT.

The study presented herein extends the simulation parameters to incorporate initial damage. Airworthiness regulations for CFRP structures require the proof of strength and the meeting of structural performance of a damaged structure with representative damage types and sizes according to the service environment [5].

A big majority of damage scenarios and their relevant compression failure mechanism that have been comprehensively investigated both theoretically and experimentally are related to impact from the stiffened panel skin side [6-9]. Stiffener damage causes more significant degradation on the structural performance of a stiffened panel. Stiffeners are degraded more if impacted from the airframe inboards space rather than from outboards. Much less was reported on the residual strength of the CFRP stiffened panel after the impact of the stiffener's edge. Recently, research efforts by [10, 11] have been targeted at elaborating the damage scenario of stiffener's edge impact and the corresponding Compression After Edge Impact (CAEI) failure mechanism.

The aim of structural optimization is to design the lightest possible structure to meet the performance requirements. This objective was heavily driven by stiffened panel failure under compressive loading and buckling. The higher the load a panel will be designed to sustain, the thicker the structural elements, hence failure will be dictated by material failure than buckling instabilities. CFRP structures have to be certified by proving their performance levels in a damaged state [5]. Damage type, size, propagation and final failure will depend on the stiffener design as well.

The numerical study presented herein, uses three stiffened panels of the same weight with an equally sized damage and investigated the compression strength degradation of each one from each original pristine state and the load carrying capacity amongst themselves. The study output aimed at proving that structural optimization for thick CFRP panels cannot be based solely on the panel buckling performance and that nonlinear finite element analysis is a valuable tool for preliminary design studies and optimal design down-selection.

2 NUMERICAL MODELLING

The study focused on providing justification for the argument that for relatively high loaded panels in compression made of CFRP materials, the optimum panel design configuration should not be based solely on its resistance to local and/or global buckling instabilities. Equally important factors are the damage initiation and propagation in the material which are affected by the material properties and design. For this reason, three stiffened panels were sought, having different stiffener configuration, as shown in figure 1.

There are many design parameters that can lead to a different panel design configuration. In this study, the base plate thickness and layup configuration was the same for all panels, as well as the stringer number. The three stringers of the same cross section for each panel and were equally spaced; two of them on the side of the panel were modelled in pristine (undamaged) condition, whereas the stringer in the middle of the panel was modelled as having a similar size delamination at the free edge. The stringer foot and top flange as well as the stringer web where of the same thickness and layup properties. The difference in the stringer design were the stringer web height and the stringer foot and top hat flange width, which were tailored accordingly for generating panels of the same weight, to the extent possible.

The pristine and damaged panels were compared in terms of the effect of edge damage on the structural behaviour under compression loading.

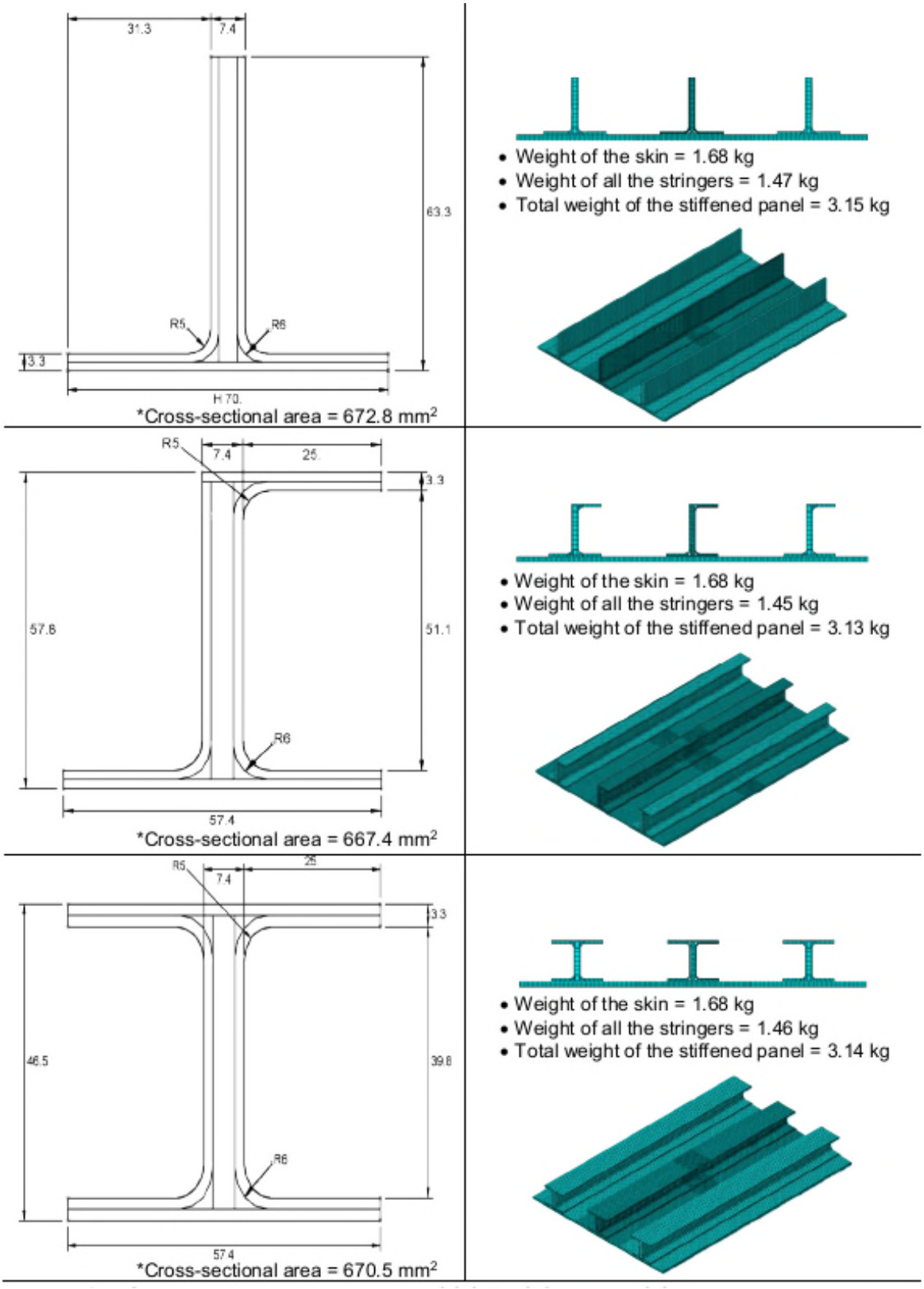

Figure 1: The three CFRP stiffened panel numerical model configurations

The inverted T-stringer panel was designed according to the specimens experimentally tested in [10] in order to

benchmark against numerical and experimental results. The other two panels, having the J and H stringers were constructed following the same numerical modelling concept in ABAQUS commercial FEA software.
The baseline stiffened panel having three equally spaced T-stringers is shown in figure 2.

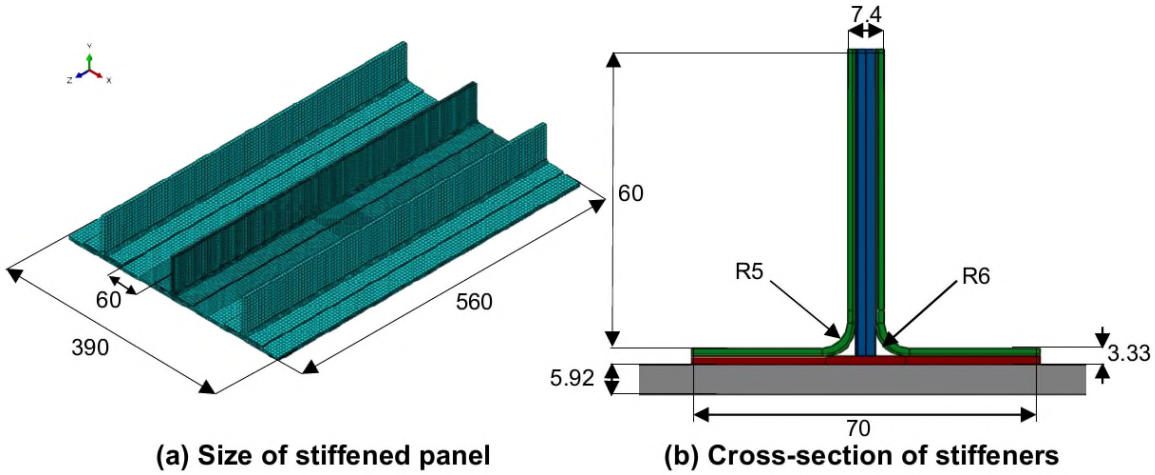

Figure 2: Baseline design of a stiffened panel with T type stringers

Reduced integration continuum shell elements 'SC8R' with enhanced hourglass control and second-order accuracy were employed for discretizing the composite laminates. Three-dimensional cohesive elements 'COH3D8' were used to discretize the cohesive layers modelled in-between certain laminates. As concluded by Li and Chen [11], based on experimental testing results, cohesive contact could be inserted only at certain interfaces that have the highest risk of delamination. These interfaces are indicated in figure 3, according to the experimental findings of reference [11]. These were four layers on the web of the T-stringer plus two more on the surface and mid-thickness of the part adhered on the plate.

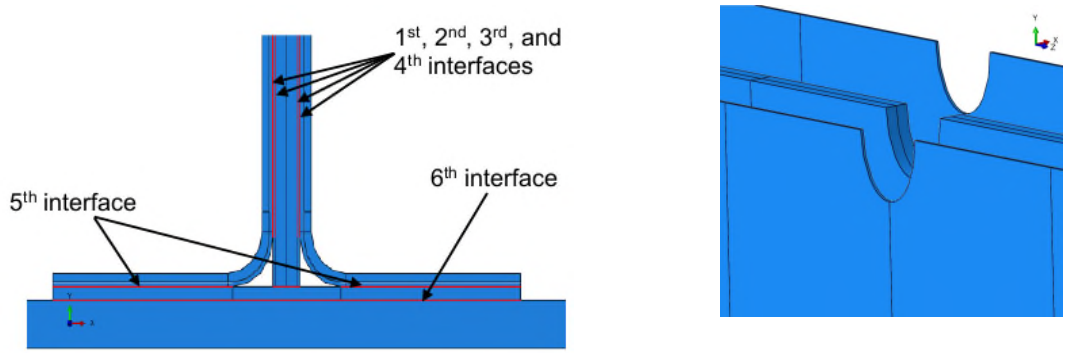

3(a) 3(b)

Figure 3: (a) Location of Cohesive Zone Modelling (CZM) layers highlighted, (b) modelled dent on the stiffener web

In the current study, the damage scenario assumed an edge impact damage, a local dent at the middle stringer along with a region of delamination was modelled. The modelling scenario assumed that a part of the stringer web (or flange) had been damaged as shown in figure 3b, while the outer layers of the web remained intact. In figure 4a, the middle part of the stringer web with the dent is shown, along with two more layers on either side also having a dent. Those layers were assembled together via a cohesive zone layer, shown in figure 3b.

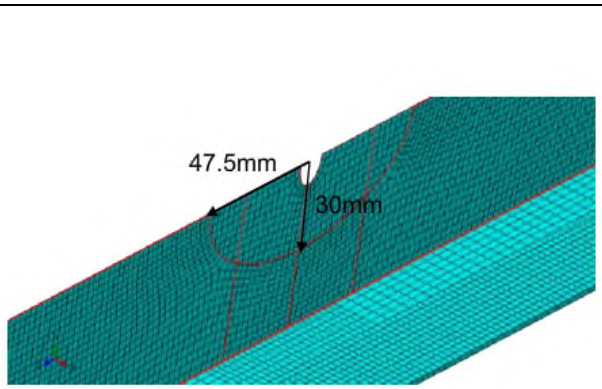

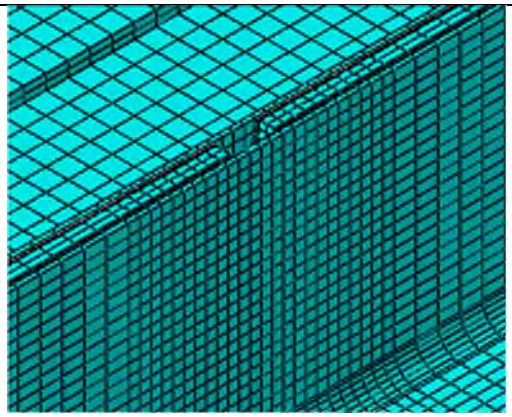

4(a) 4(b)

Figure 4: (a) Semi-elliptical delamination assumed shape, (b) damaged T-stiffener assembly

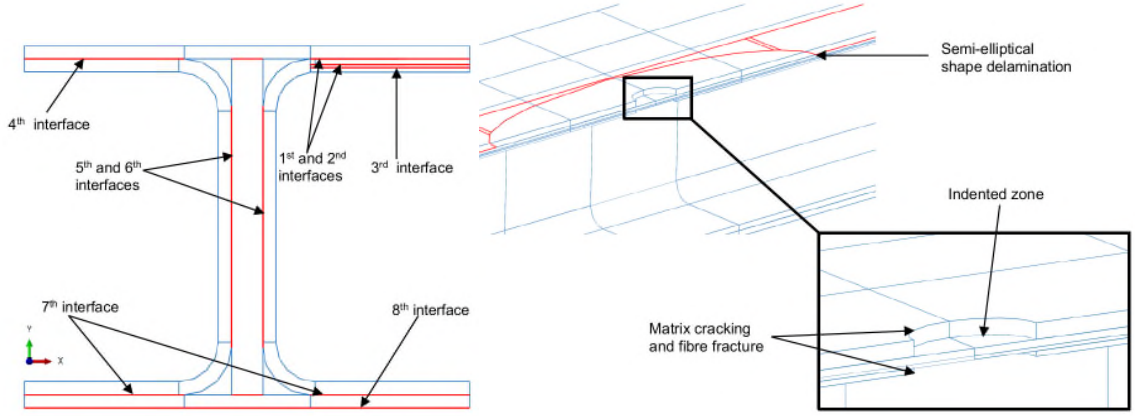

Figure 5: Damage dent and delamination modelled for the flanged stiffeners

In order to reduce the computational cost, the mesh element size was varied across the model. For the continuum shell element, locally, in the proximity of the impacted region, a refined mesh of 2.5 mm element average size was assigned, whereas, globally, a coarser mesh of 5 mm element average size was considered, as shown in figure 6. While, for the cohesive elements a refined mesh of 2.5 mm was assigned globally, without any changes in the proximity of the damage.

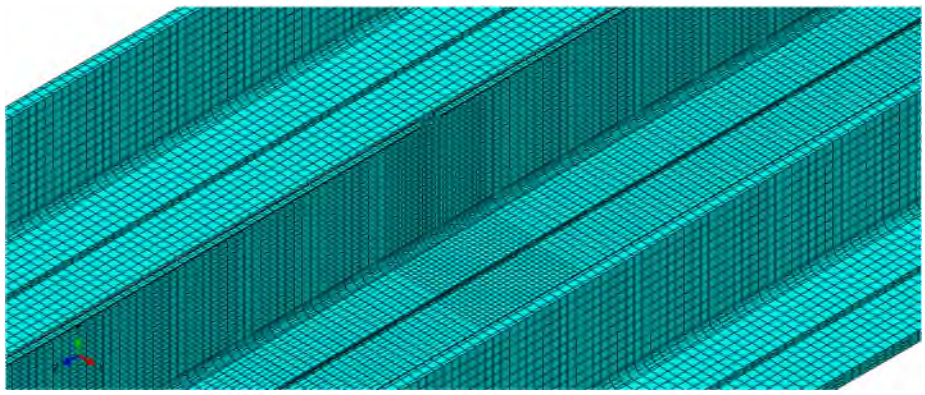

Figure 6: Mesh details in the model of T-stiffened composite panel

A mesh sensitivity study conducted in [12] by only changing the mesh element average size in the local regions of the damage showed that load vs global strain curves were not sensitive to the difference in mesh size, which are suggesting that mesh-size independent analysis can be achieved with the assigned mesh element average size of 2.5 mm.

Estimated geometric parameters for modelling the edge crushing-related region given by Li and Chen [11] are listed in

Table **1**. The width of the damage region was 5.2 mm out of 7.4 mm total thickness of the web.

Table 1 Estimated parameters for modelling edge impact damage

Symbol	Description	Value
l	Major axis of semi-elliptical (max) delamination (mm)	47.5
w	Minor axis of semi-elliptical (max) delamination (mm)	30
b_{del}	Position of maximum delamination (mm)	2.035
a	Length of the crushing damage region (mm)	10
b	Width of the crushing damage region (mm)	5.2
D_{crush}	Depth of the crushing damage region (mm)	8.3

Cohesive elements were used to model the cohesive interfaces. Figures 3 and 5, indicate the exact locations (highlighted by the red lines) where these were inserted. The material assigned for both skin and stringer is graphite fibre reinforced epoxy composite CYCOM IMS/X850 Unidirectional. Its mechanical properties from [11] are listed in table 2. In terms of the laminate layup, each ply has a thickness of 0.185 mm. The different stacking sequences of each composite laminate used in the model are listed in table 3.

Table 2: Material properties of IMS/X850 UD

Symbol	Description	Value
E_1	Longitudinal Young modulus	165 GPa
E_2	Transverse Young modulus	8.58 GPa
G_{12}	In-plane shear modulus	4.57 GPa
ν_{12}	Poisson's ratio	0.331
X^T	Longitudinal tensile strength	3071 MPa
X^C	Longitudinal compressive strength	1747 MPa
Y^T	Transverse tensile strength	88 MPa
Y^C	Transverse compressive strength	271 MPa
S_{12}	In-plane shear strength	143 MPa
τ_n^0	Cohesive nominal normal strength	39.4 MPa
τ_s^0	Cohesive nominal shear strength – 1st direction	46.1 MPa
τ_t^0	Cohesive nominal shear strength – 2nd direction	46.1 MPa
G_{Ic}	Critical Energy Release Rate ERR-Mode I	0.314 Nmm^{-1}
G_{IIc}	Critical Energy Release Rate ERR-Mode II	1.081 Nmm^{-1}
η	Power-law exponent for mixed-mode BK behaviour	2
E	Matrix Young modulus	3500 MPa
G	Matrix in-plane shear modulus	1250 MPa
$**K_N$	Penalty cohesive interface stiffness - normal direction	$3.5x10^5$ Nmm^{-3}
$**K_S,K_T$	Penalty cohesive interface stiffness - shear direction	$1.25x10^5$ Nmm^{-3}

*The values used for the cohesive strength for a mesh size of 2.5 mm.

**For the cohesive elements, the "traction-separation law" response was assigned, so the stiffness parameters do not have physical meaning and they can be estimated using a rule of thumb which says to divide the Young modulus and shear modulus of the cohesive material (epoxy) by the thickness of the cohesive element (0.01 mm);

Table 3: Ply stacking sequence and thicknesses

Components	Stacking sequence	Thickness (mm)	Colour code (see figure 2b)
Skin	[45°/90°/-45°/0_2°/-45°/0_2°/45°/0_2° /45°/0_2°/-45°/90°]s	5.92	Grey
Stringer	[45°/0°/-45°/0°/-45°/0_2°/45°/90°]s	1.665	Red
Stringer – flange	[90°/45°/0_2°/-45°/0°/-45°/0°/45°]s	1.665	Green
Stringer – web	[45°/0°/-45°/0°/-45°/0_2°/45°/90°]s	1.665	Green
Stringer – web	[90°/45°/0_2°/-45°/0°/-45°/0° /45_2°/-45°]s	4.07	Blue

Analysis boundary conditions of the panel were defined in such a way that the panel was allowed to expand only in the positive x-axis. All the nodes of the edges around the panel have restrained motion along the y-axis, as illustrated in figure 7. The lower edge nodes have restrained motion along the z-axis.

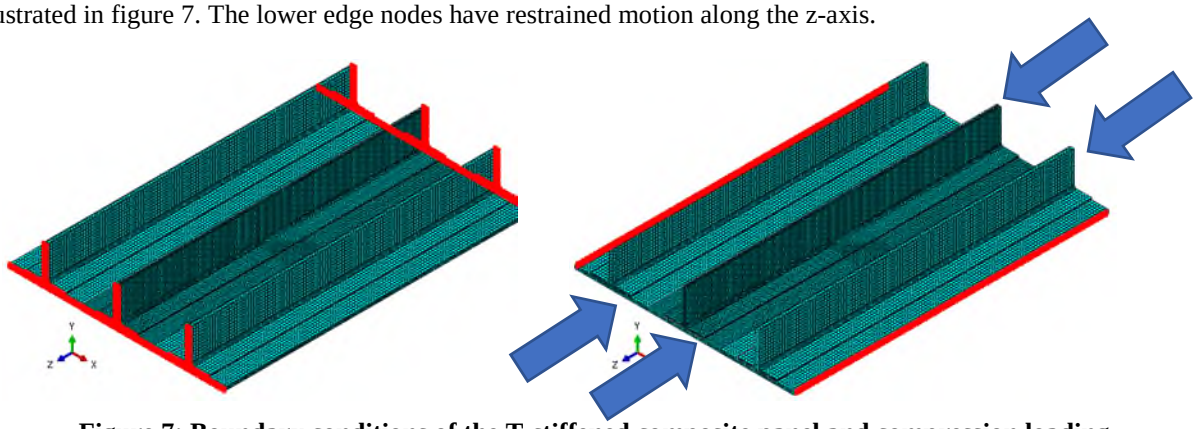

Figure 7: Boundary conditions of the T-stiffened composite panel and compression loading

A "general contact" algorithm, which comprised tangential behaviour and normal behaviour contact properties was applied between the plies to avoid unrealistic penetration; the normal behaviour property is set to default "Hard" contact for pressure-overclosure, while the tangential behaviour is set to "Frictionless" contact. Compression loading at the stiffened composite panel was applied as an in-plane displacement of the upper edge nodes towards the lower edge nodes. The total displacement applied was 4 mm.
The dynamic implicit solver is employed in this analysis. Quasi-static is a fine fit for this type of simulation as the energy dissipation (which takes place during either matrix or fibre cracking) provides extra stability and improved convergence behaviour for solving and what is essentially a final static response. Moreover, inertia effects are introduced mainly to regularize statically unstable behaviour, which may be due to unconstrained rigid body modes for a short time or "snap-through" phenomena [13].

Intra-laminar damage initiation at the composite material was assigned using 2D Hashin's damage criterion, while intra-laminar damage evolution was set up using a bilinear fracture energy-based method. The Hashin's initiation criteria formulation assigned are described by Equations **(2-1)** to **(2-4)** shown below [13]:

Fibre tension, $F_f{}^t$ $(\hat{\sigma}_{11} \geq 0)$:

$$F_f{}^t = \left(\frac{\hat{\sigma}_{11}}{X^T}\right)^2 + \alpha\left(\frac{\hat{\sigma}_{12}}{S^L}\right)^2, \qquad \textbf{(2-1)}$$

Fibre compression, $F_f{}^c$ $(\hat{\sigma}_{11} < 0)$:

$$F_f{}^c = \left(\frac{\hat{\sigma}_{11}}{X^C}\right)^2, \qquad \textbf{(2-2)}$$

Matrix tension, $F_m{}^t$ $(\hat{\sigma}_{22} \geq 0)$:

$$F_m{}^t = \left(\frac{\hat{\sigma}_{22}}{Y^T}\right)^2 + \left(\frac{\hat{\sigma}_{12}}{S^L}\right)^2, \qquad \textbf{(2-3)}$$

Matrix compression, $F_m{}^c$ $(\hat{\sigma}_{22} < 0)$:

$$F_m{}^c = \left(\frac{\hat{\sigma}_{22}}{2S^T}\right)^2 + \left[\left(\frac{Y^C}{2S^T}\right) - 1\right]\left(\frac{\hat{\sigma}_{22}}{Y^T}\right) + \left(\frac{\hat{\sigma}_{12}}{S^L}\right)^2. \qquad \textbf{(2-4)}$$

Where $\hat{\sigma}_{ij}$, the components of the effective in-plane stresses in fibre direction and normal to the fibre direction, which were used to evaluate the initiation criteria computed from $\hat{\sigma} = M\sigma$ (σ nominal stress and M is the damage operator matrix), X^T and X^C are longitudinal fibre tensile and fibre compressive strengths, Y^T and Y^C are matrix tensile and compressive strength, S^L and S^T are longitudinal and transverse shear strength, α is the coefficient which determines the contribution of the shear stress to fibre tensile initiation criterion and $\alpha = 1$ in this formulation as the model proposed in [14].

Before any type of damage initiates and propagates, the damage operator matrix M, is equal to the identity matrix, so $\hat{\sigma} = \sigma$. If damage initiation and evolution occurs for just a single mode, the damage operator matrix becomes significant in the criteria for damage initiation of other modes [13].

The damage evolution law is based on the dissipation of fracture energy during the damage progression. The decrease in material stiffness K is described according to the following equation from [13],

$$K = (1 - d_i)K_d, \quad \textbf{(2-5)}$$

where the parameter d_i is the degradation coefficient as follows from [13],

$$d_i = \frac{\delta^f_{i,eq}\left(\delta_{i,eq} - \delta^0_{i,eq}\right)}{\delta_{i,eq}\left(\delta^f_{i,eq} - \delta^0_{i,eq}\right)}; \delta^0_{i,eq} \le \delta_{i,eq} \le \delta^f_{i,eq};\ i \in (f_c, f_t, m_c, m_t), \quad \textbf{(2-6)}$$

and the equivalent displacement $\delta^f_{i,eq}$ which describes the displacement at which the material is completely damaged, and is evaluated according to the following equation from [13],

$$\delta^f_{i,eq} = \frac{2G_c}{\sigma^0_{i,eq}}, \quad \textbf{(2-7)}$$

where G_c represents the fracture energy and $\sigma^0_{i,eq}$ is the equivalent stress at which the initiation criterion of Hashin was met. From [11], the material assigned in this modelling scenario has the critical fracture energies for each mode as listed in Table 4.

Table 2 Critical Fracture Toughness properties of IMS/X850 UD

Symbol	Description	Value
G^T_{IC}	Longitudinal tensile fracture energy	133 Nmm^{-1}
G^C_{IC}	Longitudinal compressive fracture energy	10 Nmm^{-1}
G^T_{IIC}	Transverse tensile fracture energy	0.314 Nmm^{-1}
G^C_{IIC}	Transverse compressive fracture energy	1.796 Nmm^{-1}

It was important to control the way Abaqus/Implicit FE code treated elements with severe damage, since the major localised stiffness decrease could have resulted in excessive neighbouring element distortion, which in turn could cause slow-running, convergence difficulties and even early exit in the simulations. To solve potential numerical issues, severely damaged elements were not deleted from the mesh and retained some residual stiffness.

Cohesive Zone Model (CZM) was employed to numerically simulate inter-laminar delamination and to capture the damage propagation. The constitutive response assigned to the cohesive elements is based on the 'Traction-Separation law'. The Quadratic Nominal Stress Criterion (QUADS) was used to evaluate the initiation of the damage. Failure initiates when a quadratic interaction function involving a combination between the nominal and allowable stresses acting in different direction reached a value of one; the quadratic stress criterion formulation is as follows from [13],

$$\left(\frac{\tau_n}{\tau^0_n}\right)^2 + \left(\frac{\tau_s}{\tau^0_s}\right)^2 + \left(\frac{\tau_t}{\tau^0_t}\right)^2 = 1, \quad \textbf{(2-8)}$$

where τ_n, τ_s, τ_t, are the normal stress, the first and the second shear stress directions, respectively, and τ^0_n, τ^0_s, τ^0_t are the corresponding allowable stresses associated with each direction.

The following expression is employed for linear softening, which uses an evolution of the damage variable D. Its formulation is as follows, from [13],

$$D = \frac{\delta_m^f(\delta_m^{max} - \delta_m^0)}{\delta_m^{max}(\delta_m^f - \delta_m^0)}, \quad \textbf{(2-9)}$$

where $\delta_m^f = {2G^C}/{T_{eff}^0}$ is the effective traction at damage initiation and δ_m^{max} is the maximum attained effective displacement.

For the delamination growth, the Benzeggagh-Kenane (BK) mixed mode behaviour criterion was used with mode mix ratio based on energy. The criterion can be represented as follows, from [13],

$$G_C = G_{Ic} + (G_{IIc} - G_{Ic})\left(\frac{G_{II} + G_{III}}{G_I + G_{II} + G_{III}}\right)^{\eta}, \quad \textbf{(2-10)}$$

where G_C is the mix-mode fracture energy rate, G_{Ic} and G_{IIc} are the critical ERR for Mode I and Mode II, respectively; G_I, G_{II}, G_{III} are associated with the work done the traction and its relative displacement in the normal direction, and the first and the second shear directions, respectively; η refers to the mixed-mode interaction and it was experimentally determined by [11] to have a specific value of 2.

As previously discussed, to avoid numerical issues, it is equally applicable to the cohesive elements that any element that reaches complete failure shall retain some residual stiffness ($d_{max} = 0.99$) and the element shall not be deleted from the mesh. In Abaqus/Implicit FE code the material models employ softening behaviour and stiffness degradation, which frequently lead to convergence difficulties. A common technique used to overcome these convergence difficulties is by employing viscous regularization. The traction-separation laws used to describe the constitutive behaviour of the cohesive elements was regularized using a viscosity coefficient of 10^{-3} to help to bypass convergence difficulties in the non-linear region. This value was selected as a result of surveying the published data, consulting the documentation of Abaqus [13] (which states that 10^{-4} matched experimental results for displacement values greater than 20mm) and various simulation trials, which showed that, in this modelling scenario, this magnitude is a fine balance between accurate enough results and avoiding excessive deceleration in the time that it takes for a simulation to converge.

3 RESULTS AND DISCUSSION

The compression load versus displacement results for the three panels, in their pristine and damaged conditions, are shown in figure 9. The results show that the J and H stiffened pristine panels, can attain an almost identical load in compression (2762 and 2761N respectively), higher than the T stiffened panel (2628N). More importantly though, is the percentage decrease in the strength for the damaged panels with respect their undamaged state; for the J and H stiffened panels, the reduction in their compression strength measured was about 20%, while for the T stiffened panels, was approximately 35%.

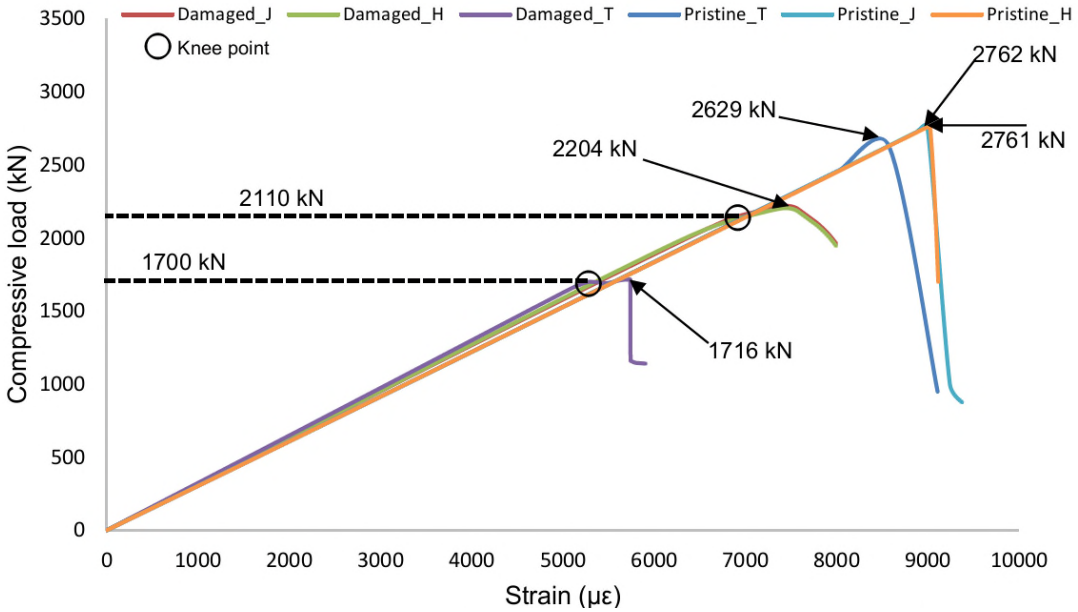

Figure 9: Compression load versus displacement curves for the three panel design configurations with T, J and H stringers. Results for pristine (undamaged) and damaged state

Figure 10 shows the deformation shapes and locations of maximum compressive failure along the fibre direction of the laminate layup. The damage pattern for the J and H stiffened panels was similar, different to the T stiffened one. The stiffeners of the J and H panels experience more widespread fibre failure on the top flange of the stiffeners, indication to their higher load carrying capacity and different loading ratio between the baseplate and the stiffeners. The horizontal cracks on the baseplate are spaced more closely for the J and H stiffened panels, indication of a higher buckling eigenvalue.

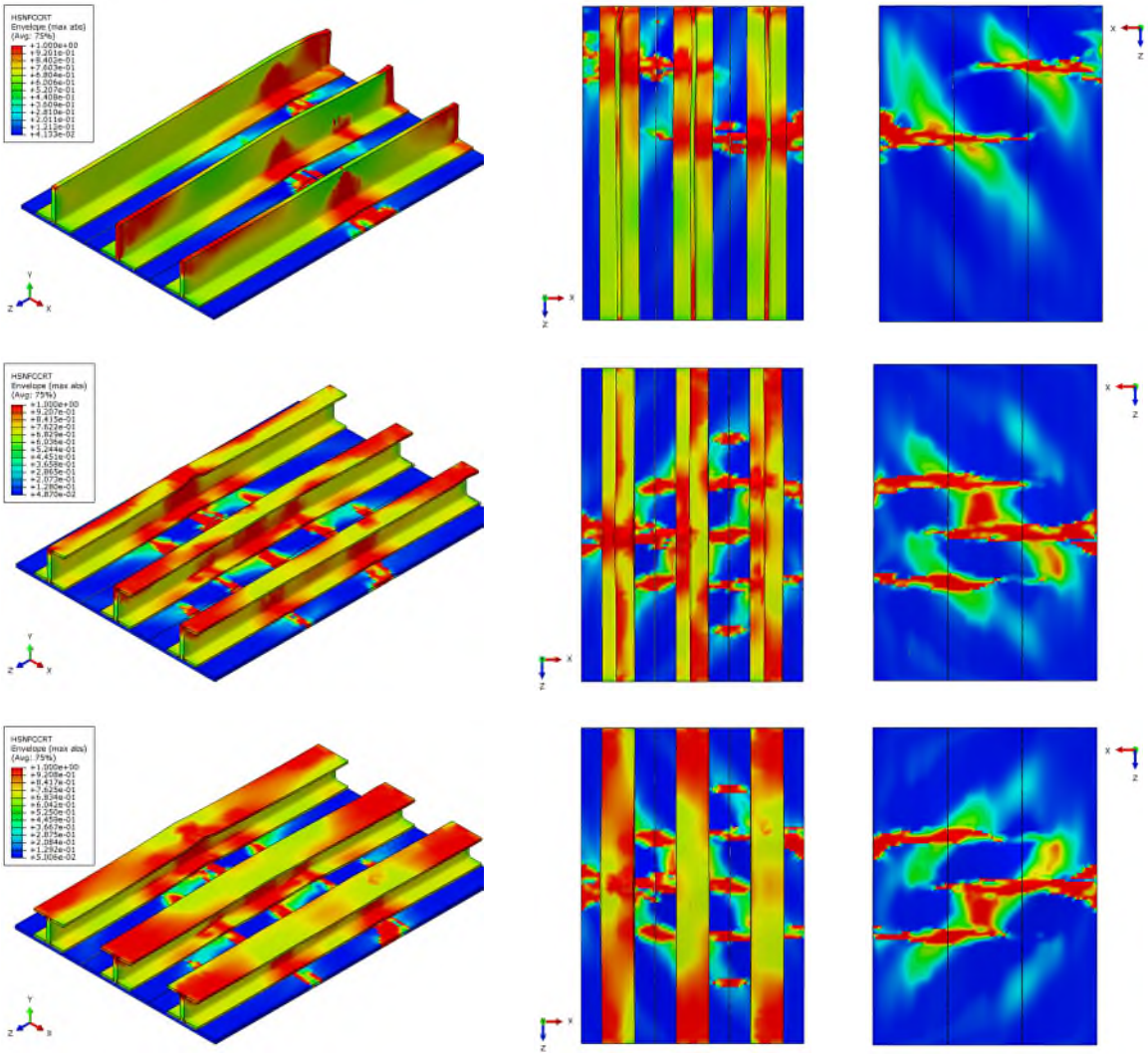

Figure 10: Fringe plot showing material fibre failure in compression superimposed on the deformation of pristine panels

For the damaged panels, damage propagated from the assumed damaged position in the middle stiffener for all panels, as shown in figure 11. The images in figure 12 show the damage propagation at the cross section of the assumed damage, in terms of fibre compression failure and delamination of the cohesive boundary.

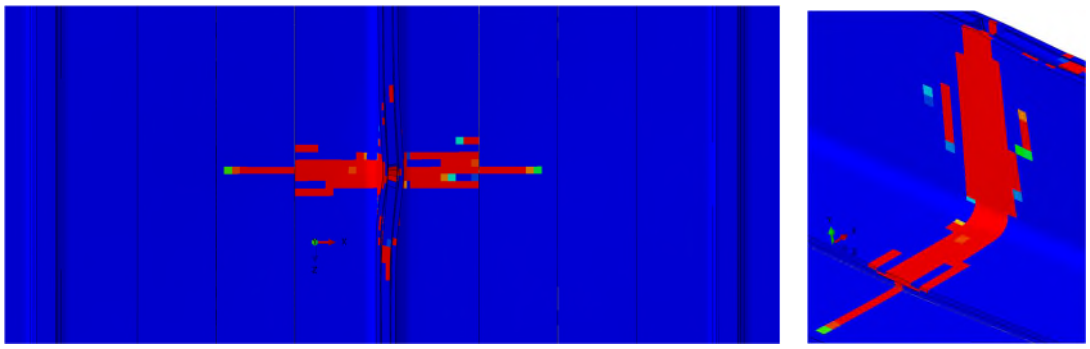

Figure 11: Damage propagating from the assumed middle stringer location, extending perpendicular to the loading direction (T-stiffened panel shown)

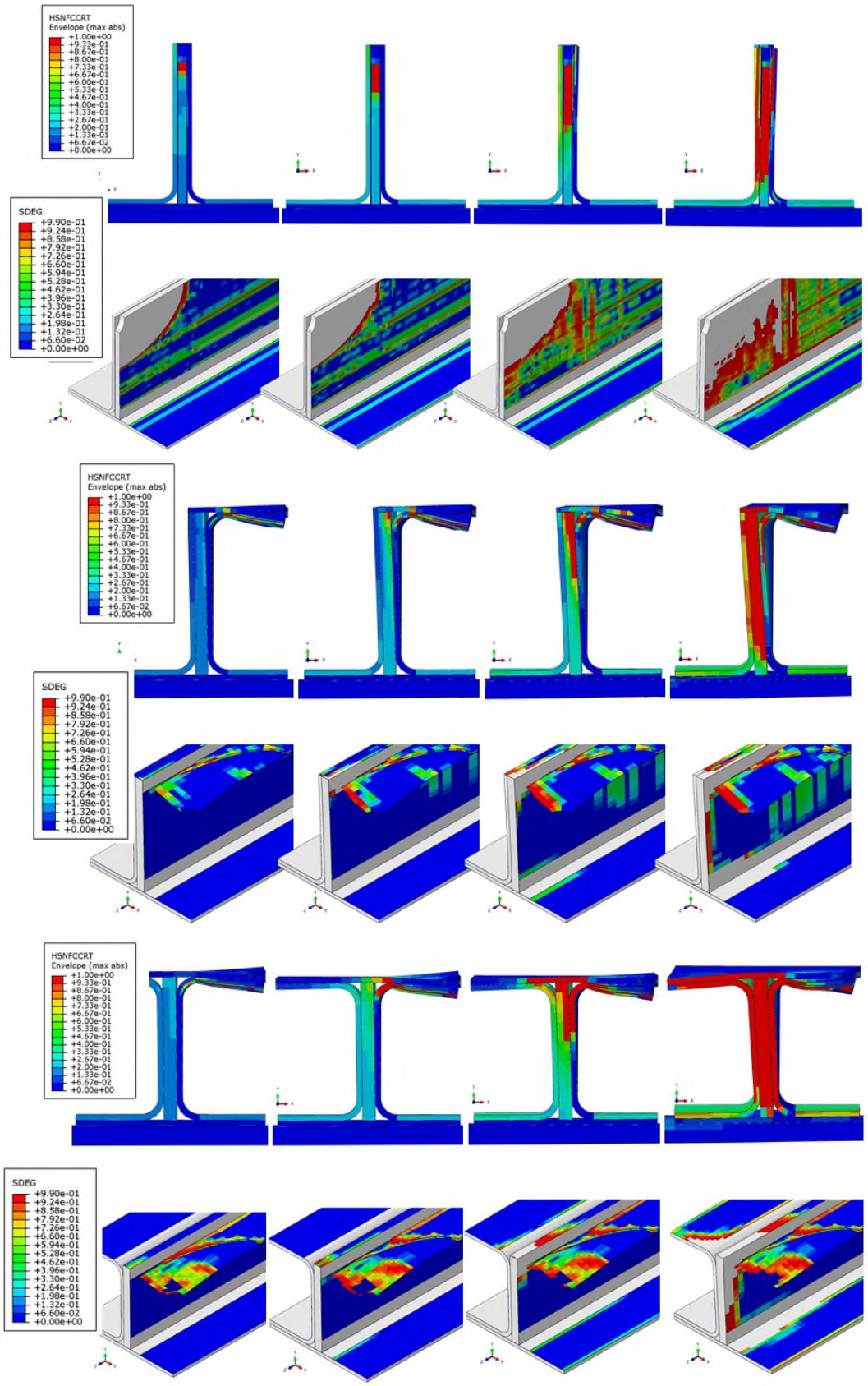

Figure 12: Damage propagation in terms of fibre compression (rows 1, 3 and 5) and cohesive layer delamination (rows 2, 4 and 6) for the three panels, at various loading stages during simulation

4 CONCLUSIONS

In the current study, three CFRP stiffened panels, with similar damage sizes where put to the test. The J and H stiffened panels, although having different bending stiffness, they resulted in a very similar ultimate load capability, while the T stiffened panel, having the biggest bending stiffness, collapsed earlier and with a higher percentage load drop form its pristine condition.

The study aimed at highlighting that for highly loaded stiffened CFRP panels, it is not just the panel's elastic stability behaviour that will determine the optimal design parameters set for better structural performance; the material properties in terms of strength and fracture toughness as well as the specific structural design detail, will control the overall structural performance.

More importantly, and since for CFRP structures in the aerospace sector have to exhibit certain levels of strength while being damaged, it is the percentage in the strength reduction that will dictate the optimal structural configuration.

REFERENCES

[1] Smith, F. (no date a) The use of composites in aerospace: past, present and future challenges. Available at: https://avaloncsl.files.wordpress.com/2013/01/avalon-the-use-of-composites-in-aerospace-s.pdf (Accessed: 1 August 2018).
[2] Zimmermann, R. and Rolfes, R. (2006) 'POSICOSS - Improved postbuckling simulation for design of fibre composite stiffened fuselage structures', Composite Structures, 73(2), pp. 171–174. doi: 10.1016/j.compstruct.2005.11.041.
[3] Degenhardt, R., Rolfes, R., Zimmermann, R. and Rohwer, K. (2006) 'COCOMAT - Improved material exploitation of composite airframe structures by accurate simulation of postbuckling and collapse', Composite Structures, 73(2), pp. 175–178. doi: 10.1016/j.compstruct.2005.11.042.
[4] EASA. Certification specifications and acceptable means of compliance for large aeroplanes CS-25. Amend 17; 2017.
[5] EASA. Acceptable Means of Compliance – Composite Aircraft Structure AMC 2029; 2010.
[6] Rivallant, S., Bouvet, C., Abi Abdallah, E., Broll, B. and Barrau, J. J. (2014) 'Experimental analysis of CFRP laminates subjected to compression after impact: The role of impact-induced cracks in failure', Composite Structures, 111(1), pp. 147–157. doi: 10.1016/j.compstruct.2013.12.012.
[7] Rhead, A. T. and Butler, R. (2009) 'Compressive static strength model for impact damaged laminates', Composites Science and Technology, 69(14), pp. 2301–2307. doi: 10.1016/j.compscitech.2009.01.010.
[8] Esrail, F. and Kassapoglou, C. (2014) 'An efficient approach to determine compression after impact strength of quasi-isotropic composite laminates', Composites Science and Technology, 98, pp. 28–35. doi: 10.1016/j.compscitech.2014.04.015.
[9] Masood, S. N., Vishakh, R., Viswamurthy, S. R., Gaddikeri, K. M. and Sridhar, I. (2018) 'Influence of stiffener configuration on post-buckled response of composite panels with impact damages', Composite Structures, 194(January), pp. 433–444. doi: 10.1016/j.compstruct.2018.04.005.
[10] Ostré, B., Bouvet, C., Lachaud, F., Minot, C. and Aboissière, J. (2015) 'Edge impact damage scenario on stiffened composite structure', Journal of Composite Materials, 49(13), pp. 1599–1612. doi: 10.1177/0021998314537325.
[11] Li, N. and Chen, P. (2017) 'Failure prediction of T-stiffened composite panels subjected to compression after edge impact', Composite Structures. Elsevier Ltd, 162, pp. 210–226. doi: 10.1016/j.compstruct.2016.12.004.
[12] Li, N. and Chen, P. (2017) 'Prediction of Compression-After-Edge-Impact (CAEI) behaviour in composite panel stiffened with I-shaped stiffeners', Composites Part B: Engineering, 110, pp. 402–419. doi: 10.1016/j.compositesb.2016.11.043.
[13] 'Abaqus V6.14. Documentation' (2014). ABAQUS, Inc. 2014.
[14] Hashin, Z. (1980) 'Failure Criteria for Unidirectional Fiber Composites', Journal of Applied Mechanics, 47(2), p. 329. doi: 10.1115/1.3153664.